buildings

MDPI

Article

Flexural Behaviour of Built-Up Beams Made of Optimised Sections

Elilarasi Kanthasamy [1,*], Janaid Hussain [1], Kajaharan Thirunavukkarasu [2], Keerthan Poologanathan [1], Krishanu Roy [3], G. Beulah Gnana Ananthi [4] and Thadshajini Suntharalingam [5]

1 Faculty of Engineering and Environment, Northumbria University, Newcastle upon Tyne NE1 8ST, UK
2 Institute of Technology, University of Moratuwa, Homagama 10200, Sri Lanka
3 School of Engineering, University of Waikato, Hamilton 3240, New Zealand
4 Department of Civil Engineering, College of Engineering Guindy Campus, Anna University, Chennai 600025, India
5 School of Computing, Engineering, and Digital Technologies, Teesside University, Middlesbrough TS1 3BX, UK
* Correspondence: elilarasi.kanthasamy@northumbria.ac.uk

Abstract: The modular construction industry often seeks cost-effective, high-performing, and longer-span members in buildings to ensure efficiency and quality. Accordingly, the idea of built-up sections was brought into gain numerous benefits including higher structural capacity, improved torsional rigidity, and increased stiffness. While limited research studies have been carried out to study the structural performances of built-up sections, few innovative section profiles have been developed in the industry considering the structural benefits, including improved stiffness. Hence, the application of newly developed built-up sections could enhance the employment of built-up sections in the industry. On that note, this research is focused on the flexural behaviour of optimised section profiles named the LCB-benchmark (Lipped Channel Beam), the optimised-LCB, folded-flange and the super-sigma sections. In addition, different materials, namely cold-formed carbon steel (CFS), cold-formed (CF) aluminium and CF stainless steel, were considered for built-up sections, in order to provide recommendations based on their flexural performances. Numerical analysis was carried out on single sections as well as on built-up sections to the developed parametric plan after the successful validation of experimental studies. The results were compared for single and built-up sections. Finally, based on the comparisons, the folded-flange built-up section is recommended for all three materials as it displayed the highest bending capacity, and the capacity enhancement compared to the corresponding single section was a minimum of 131%.

Keywords: flexural behaviour; built-up section; cold-formed steel; stainless steel; aluminium; numerical analysis

Citation: Kanthasamy, E.; Hussain, J.; Thirunavukkarasu, K.; Poologanathan, K.; Roy, K.; Beulah Gnana Ananthi, G.; Suntharalingam, T. Flexural Behaviour of Built-Up Beams Made of Optimised Sections. *Buildings* **2022**, *12*, 1868. https://doi.org/10.3390/buildings12111868

Academic Editors: Edoardo M. Marino and Bo Yang

Received: 3 September 2022
Accepted: 31 October 2022
Published: 3 November 2022

1. Introduction

Built-up sections were introduced to the building industry, especially to the CFS sector, to address the demand for higher structural capacity members in mid-rise residential buildings and industrial structures, in order to achieve the design loads which are not attained by the standard single sections. Built-up sections are assembled by combining two or more single sections using fastening components such as clinches, welds, bolts and self-tapping screws [1–3]. The assembly of built-up sections can be carried out either back-to-back or as a nested box-type section, as illustrated in Figure 1, considering the design requirements as well as the applications. The utilisation of built-up sections in the structural applications is highly considered because of advantages such as flexibility in introducing different doubly symmetric shapes, improved stiffness, higher strength and enhanced torsional rigidity [4–6]. Hence, built-up sections are now being considered in the design process of modular buildings where higher capacity and maximised spanning distance are required [7]. In addition, the sustainability aspects of built-up sections are

rated highly in relation to cost, material efficiency, improved structural performance and aesthetic values [7]. Furthermore, introducing different innovative cross-sections in the CFS industry such as SupaCee, Sigma, LiteSteel Beam (LSB), Diamond Hi-Span (DHS), Ultra BEAM, Albion Sigma beam, King span and Super-Sigma [8–12], has paved the way for experimenting with different built-up sections.

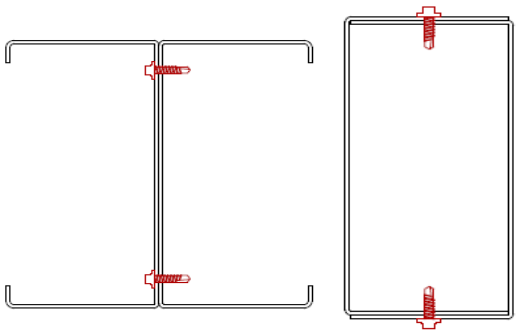

(**a**) (**b**)

Figure 1. Built-up section common profiles: (**a**) Open built-up section; (**b**) Closed built-up section (Box type) [12].

Numerous research studies have been carried out to study the structural capacities of various built-up sections under bending, web crippling and shear, considering different materials such as CFS, CF aluminium and CF stainless steel. Wang and Young [13] investigated the flexural behaviour of open and closed CFS channel built-up sections. The study predicted that screw spacing does not have much effect for open built-up section while it influences the flexural capacity of close built-up sections significantly. The same researchers [1,2] presented a comprehensive experimental and numerical analysis of the flexural performance of five different CFS built-up section profiles with intermediate stiffeners. Subsequently, Anbarasu [14] investigated the flexural behaviour of closed CFS built-up beams composed of sigma sections. Meanwhile, Ye et al. [15] focussed on back-to-back connected open built-up beams composed of LCBs and studied the flexural performance using experimental and numerical approaches. In addition, Jeyaragan and Mahendran [16] conducted a numerical investigation of back-to-back built-up LiteSteel Beam (LSB) to study the flexural performance. It was concluded that 2.12 to 2.16 times the capacity enhancement was evident compared to individual sections for a span of 2 m and the ratio increased up to 2.55 for a span of 4 m. In addition, Jeyaragan and Mahendran [16] pointed out that the spacing between self-tapping screws influences the bending capacity of built-up sections. A similar statement based on more data was made by Kajaharan et al. [7] when they compared the flexural capacity of both open and closed built-up sections with different screw spacing. However, Xu et al. [17] reported that the bending capacity of closed CFS built-up sections can be predicted by the summation of the individual sections' (C-section and track section) flexural capacity for concentric loading and the addition of individual sections' flexural strength with the modification factor of 0.9 for eccentric loading, respectively.

Wang et al. [18] carried out experimental and numerical studies on perforated channel built-up sections using aluminium alloys. The study was conducted for a four-point and three-point bending set-up. In terms of stainless steel, flexural behaviour of ferritic stainless steel built-up sections was conducted by Karthik and Anbarasu [19]. The researchers conducted numerical analyses for closed built-up sections made of lipped channel sections.

A number of innovative section profiles are yet to be studied in the context of built-up sections. Gatheeshgar et al. [11] carried out optimisation studies for CFS members to acquire enhanced flexural capacities. The researchers conducted an optimisation study using particle swarm optimisation (PSO) for CFS sections such as folded-flange, super-sigma and optimised-LCB sections by considering a similar amount of material with a benchmark LCB section which is commercially available. The effective width method described in

EN1993-1-3 (EC3) [20] was adopted to determine the section moment capacities of those sections. In addition, web crippling and the shear behaviour of the optimised sections were also determined using numerical analyses. Therefore, this paper intends to extend their study and to report the flexural behaviour of built-up sections composed of those benchmarked cross-sections, folded-flange, optimised-LCB and super-sigma, as illustrated in Table 1. Optimised-LCB was derived from the optimisation studies of benchmark LCB section, which varies in dimension only. In addition, different materials, including CFS, CF aluminium and CF stainless steel, were considered to widen the research applications, considering the beneficial aspects of those materials in the construction industry.

Table 1. Optimised single and built-up sections.

Prototypes	Single Sections [11]	Built-Up Sections
Benchmark or Optimised-LCB	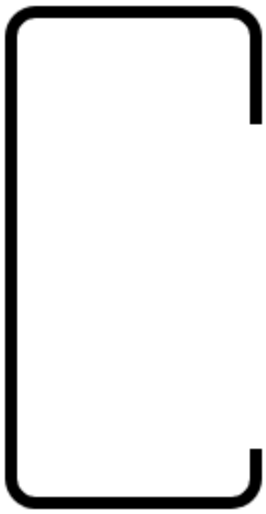	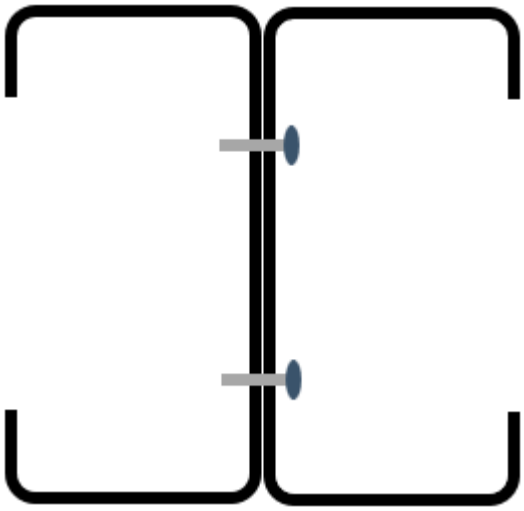
Folded-Flange		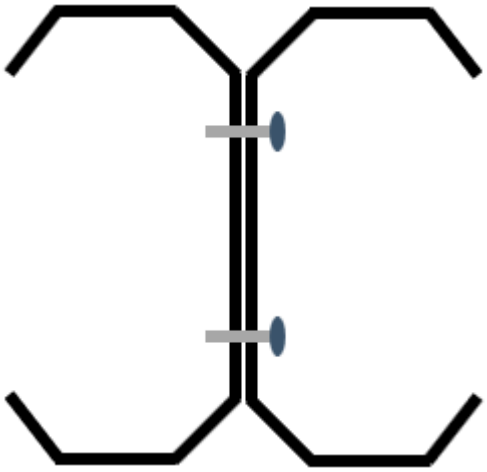

Table 1. *Cont.*

Prototypes	Single Sections [11]	Built-Up Sections
Super-Sigma	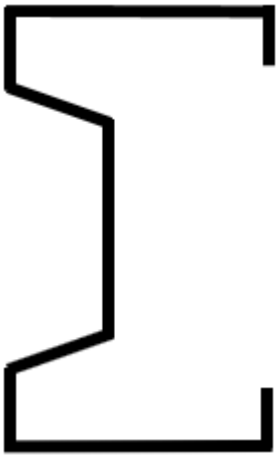	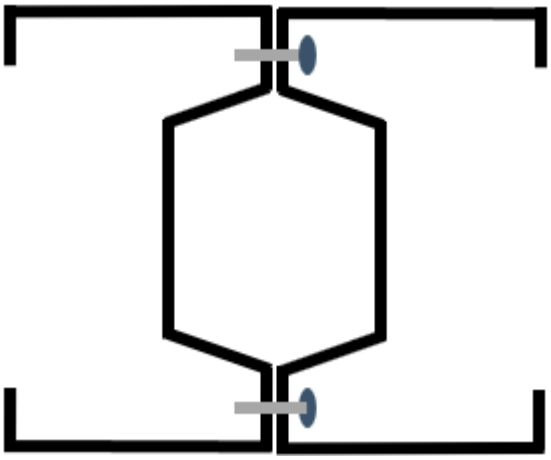

2. Finite Element Modelling

2.1. Finite Element Type and Mesh

Numerical models of built-up sections and single sections were generated by adopting the finite element software ABAQUS, version 2020 [21]. Initially, experimental tests of flexural behaviour of built-up lipped channel sections and several innovative sections with stiffened web were validated. The four-point bending set-up with pin and roller supports was used in this study. Figure 2 shows a schematic diagram of a four-point loading set-up with the corresponding numerical model. Finite element analysis was conducted to compare their structural capacities among optimised cross-sections and to investigate the increment in built-up sections over their single sections in terms of flexural capacity.

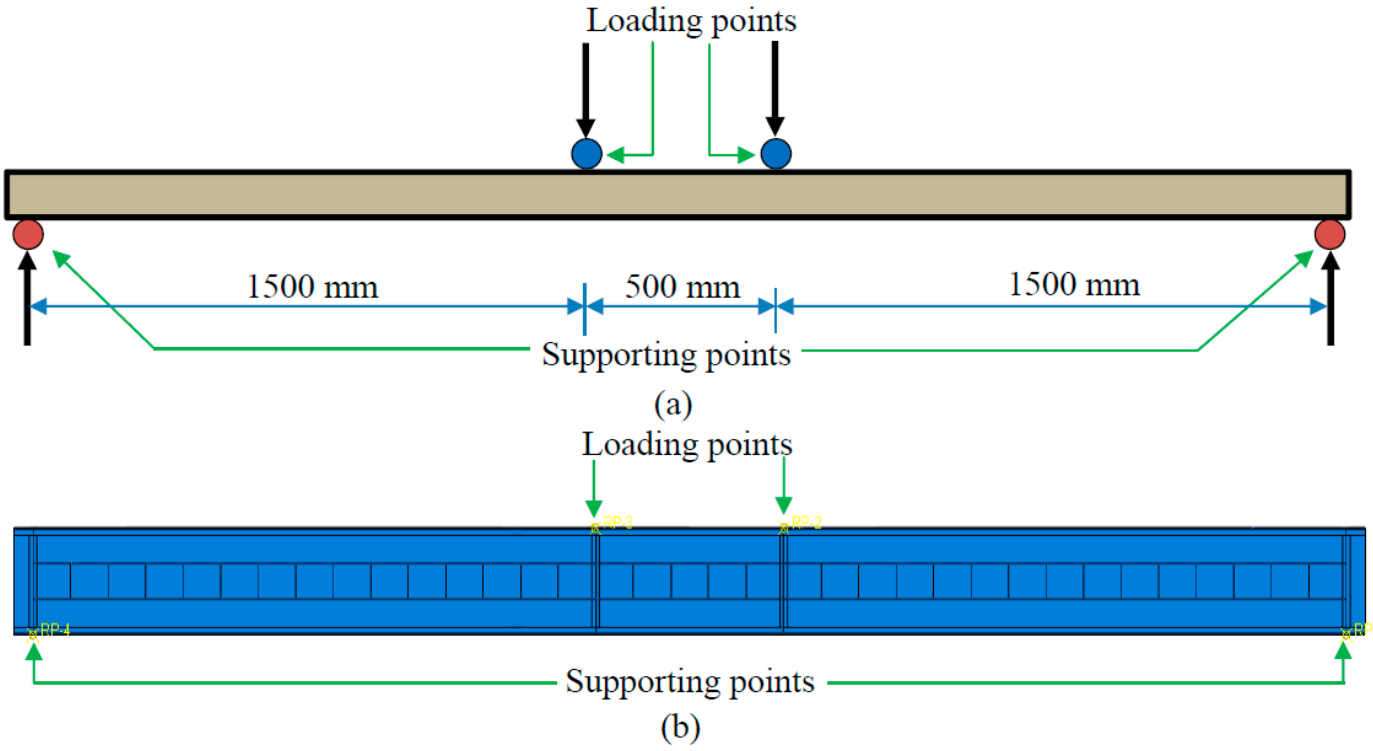

Figure 2. Four-point bending set-up (**a**) Schematic diagram and (**b**) Numerical model.

The CFS sections were modelled using the S4R element, which is a four-node quadrilateral shell element, whilst loading and supporting plates were generated with the R3D4 element. Mesh sensitivity analysis was performed for proper mesh application to represent the flexural behaviour of CFS sections accurately. Finally, 5 mm × 5 mm and 5 mm × 1 mm mesh sizes were adopted to the flat and corner portions of the beam, respectively. However, web side plates, which are used for loading and supporting plates in the single section, were meshed with 10 mm × 10 mm, which does not have much influence on the analysis. The applied meshing scheme for both the single and built-up sections is shown in Figure 3. Similar element models and meshing scheme were also noticed in the previous numerical studies [22–24].

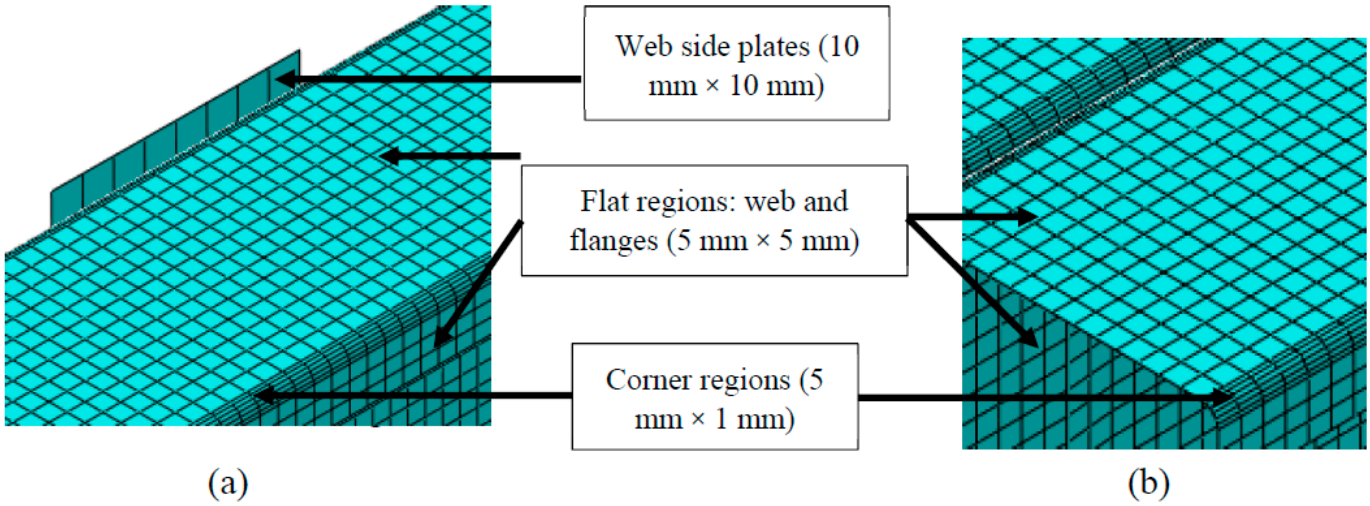

Figure 3. Meshing scheme (**a**) Single sections and (**b**) Built-up sections.

2.2. Material Modelling

Three different materials, namely CF carbon steel, CF aluminium, and CF stainless steel, were considered in this study. However, all three materials were assigned with one similar material yield strength for comparative purposes. Material grades adopted in numerical analyses are outlined in Table 2. Density, modulus of elasticity, and Poisson's ratio of all materials are also illustrated in Table 2.

Table 2. Selected material properties for the parametric study.

Material	Material Strength (MPa)	Density (Kg/m^3)	Young's Modulus (MPa)	Poisson's Ratio
CF carbon steel	f_y = 220	7850	210,000	0.30
	f_y = 450			
CF aluminium	5052-H14 (f_y = 180, f_u = 230)	2700	70,000	0.33
	3004-H48 (f_y = 220, f_u = 260)			
CF stainless-steel	1.4307 (f_y = 220, f_u = 520)	7850	210,000	0.30
	1.4362 (f_y = 450, f_u = 650)			

The material model of CFS was delineated using a bilinear model with nominal yield strength in Abaqus, as illustrated in Figure 4. Moreover, Young's modulus, Poisson's ratio, and density of the CFS were assigned to the FE modelling. All the material properties that were used for CFS are given in Table 2.

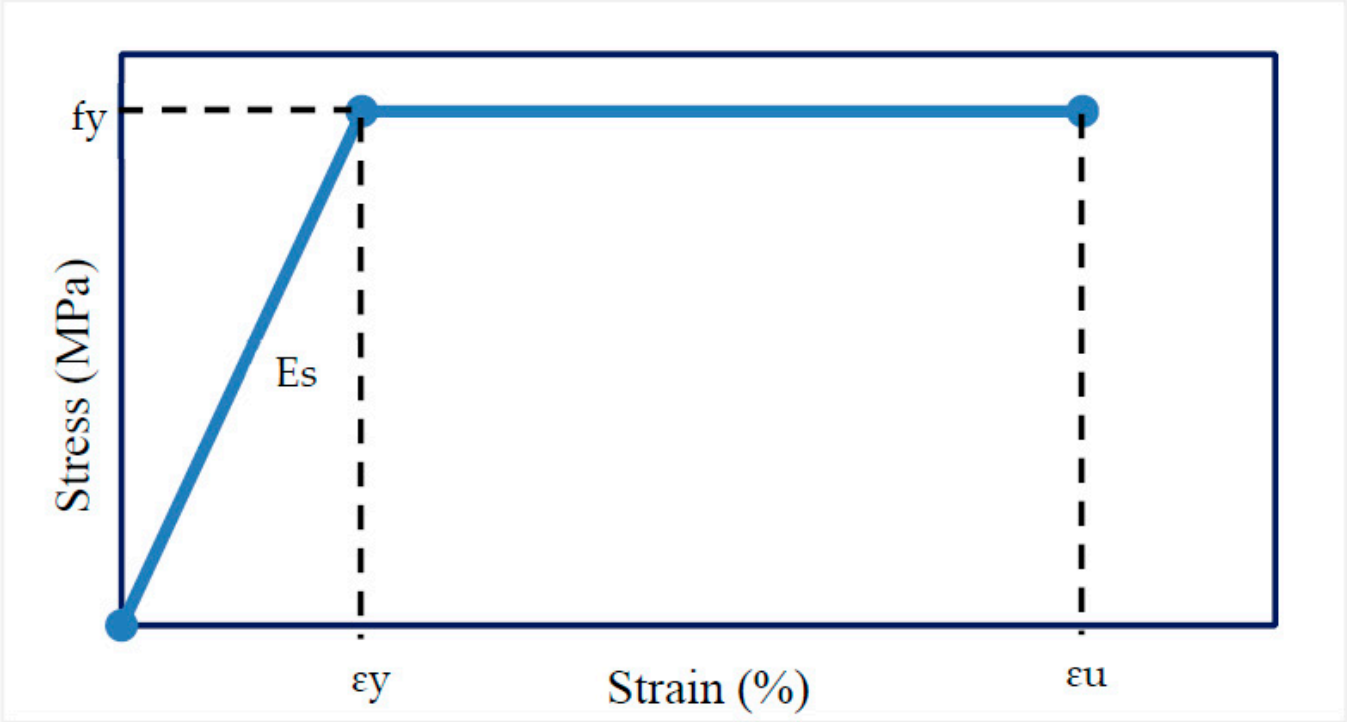

Figure 4. Typical stress-strain curve of CFS.

The material model for the CF aluminium was derived using the continuous strength method (CSM) developed by Su et al. [25]. The material model comprises two segments: elastic region and linear hardening region. The elastic and linear hardening parts were derived using Young's modulus (E) and strain hardening slope (E_{sh}), respectively. The bilinear CSM material model is shown in Figure 5, whilst the equations used in this study to derive this material model are illustrated in Equations (1) and (2). The same material model was also employed by some other researchers [26,27].

$$E_{sh} = \frac{f_u - f_y}{C_2\varepsilon_u - \varepsilon_y} \tag{1}$$

$$\varepsilon_u = C_3\left(1 - \frac{f_y}{f_u}\right) + C_4 \tag{2}$$

where, E_{sh}—strain hardening modulus, ε_y—yield strain, ε_u—ultimate strain, f_y—yield strength, f_u—ultimate strength, $C_2 = 0.5$, $C_3 = 0.13$ and $C_4 = 0.059$

Two-stage Ramberg-Osgood model which was recently modified by Rasmussen [28] adopted to represent the stress-strain behaviour of the CF stainless steel section. The material model is developed with elastic and non-linear strain hardening regions. The equations used to develop the full stress-strain curve of the CF stainless steel materials are given in Equations (3) and (4). The stress-strain curve for CF stainless steel material is derived using Equations (3) and (4) and was then converted to true stress and plastic strain values to be adopted in the ABAQUS.

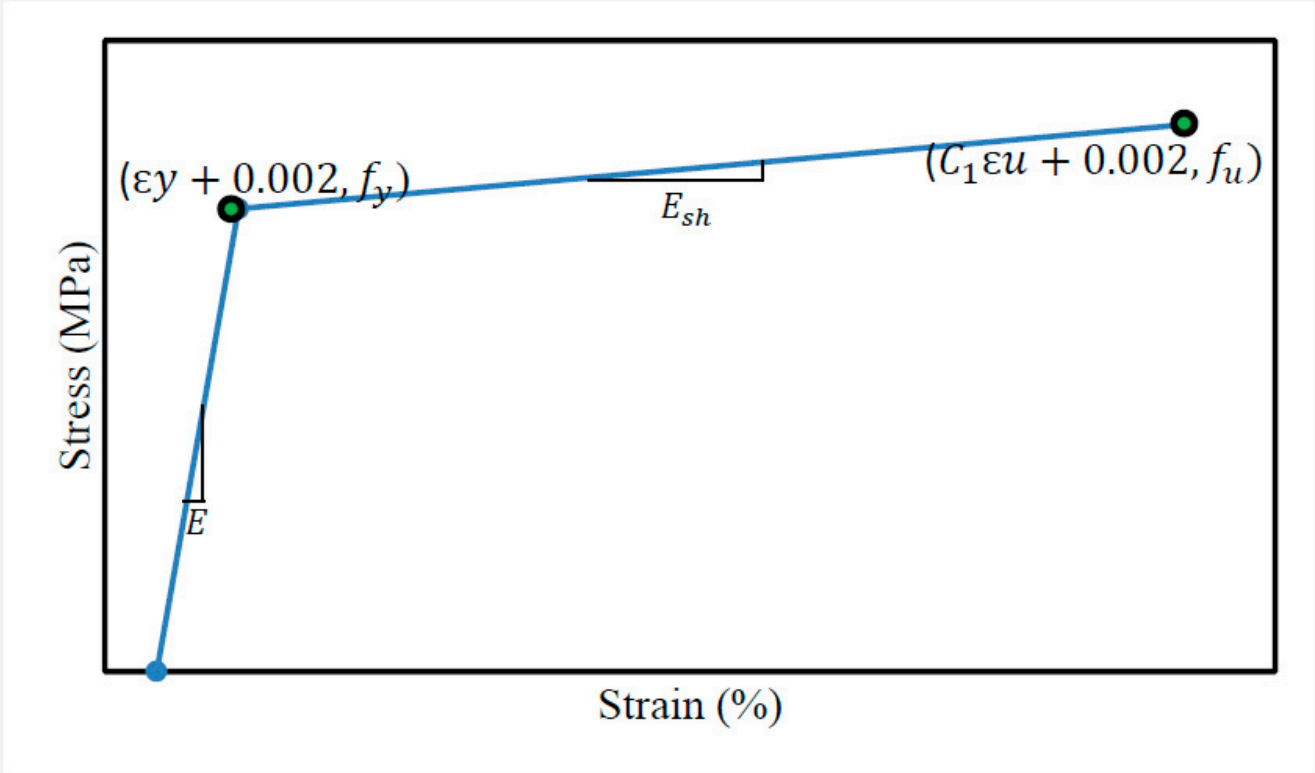

Figure 5. Material model curve of CF aluminium-Continuous Strength Method (CSM).

$$\varepsilon = \frac{\sigma}{E_0} + 0.002\left(\frac{\sigma}{\sigma_{0.2}}\right)^n \; for\; \sigma \leq \sigma_{0.2} \tag{3}$$

$$\varepsilon = \varepsilon_u + \frac{\sigma - \sigma_{0.2}}{E_{0.2}} + \varepsilon_u\left(\frac{\sigma - \sigma_{0.2}}{\sigma_u - \sigma_{0.2}}\right)^m \; for\; \sigma > \sigma_{0.2} \tag{4}$$

where, E_0—initial elastic modulus or Young's modulus, σ_u—ultimate stress, ε_u—ultimate strain, $\sigma_{0.2}$—proof stress corresponding to 0.2% of plastic strain, $\varepsilon_{0.2}$—total strain at 0.2% proof stress and $E_{0.2}$—elastic tangent modulus at 0.2% proof stress.

Moreover, material strength enhancement was considered in the corner regions of the CF stainless steel sections, whilst the above-mentioned material model was applied in the flat regions. Plastic deformation occurs in the corner regions of the CF stainless-steel sections during the fabrication processes [27]. Research studies identified huge plastic deformation in the corner regions of CF stainless steel sections and proposed material model equations. The expressions are available to predict the 0.2% proof stress and ultimate stress of the corner regions, shown in Equations (5) and (6) [29,30].

$$\sigma_{0.2,pb,c} = \frac{1.673\sigma_{0.2,mill}}{\left(\frac{r_i}{t}\right)^{0.126}} \tag{5}$$

$$\sigma_{u,pb,c} = 0.75\sigma_{0.2,c}\left(\frac{\sigma_{u,mill}}{\sigma_{0.2,mill}}\right) \tag{6}$$

where, $\sigma_{0.2,pb,c}$—0.2% proof stress at corner region, $\sigma_{u,pb,c}$—ultimate stress of the corner regions, r_i—internal corner radius, t—thickness, $\sigma_{0.2,\,mill}$—0.2% proof stress given in mill certificate and $\sigma_{u,\,mill}$—ultimate stress given in the mill certificate.

2.3. Loading and Boundary Conditions

In the experimental set-up, loads and supporting forces were applied using load transfer plates, which was replicated in the numerical model in a simplified way. Surfaces

corresponding to the loading and supporting regions coupled to a reference point. The surfaces are flange and web of the beam which are connected to the bearing plates and stiffener plates respectively according to the experimental setup (Figure 6). Therefore, altogether there were four coupled regions (Figure 6) which were coupled individually to their corresponding reference points, and boundary conditions were then applied to those corresponding reference points. Also, the loading was applied using displacement control. Supporting boundary conditions were defined to be pin and roller supports. In addition, both top and bottom flanges were laterally restrained at 300 mm interval to ensure the local buckling behaviour in this study. All the loading and supporting boundary conditions applied to the built-up section is shown in Figure 6. For single sections, boundary conditions were applied using web side plates, delineated in Figure 7.

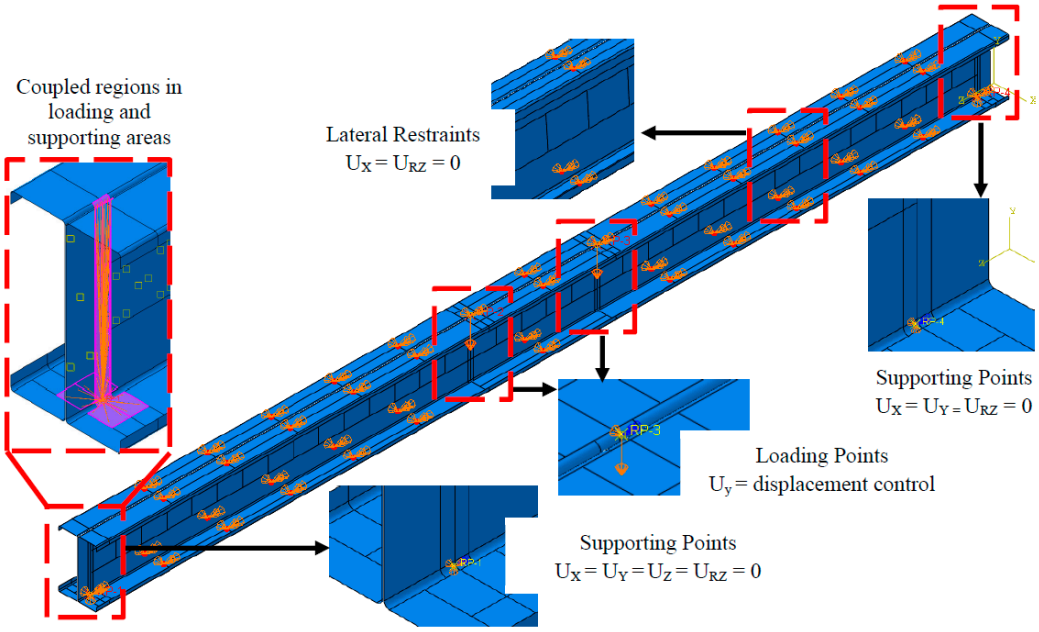

Figure 6. Boundary conditions of built-up sections.

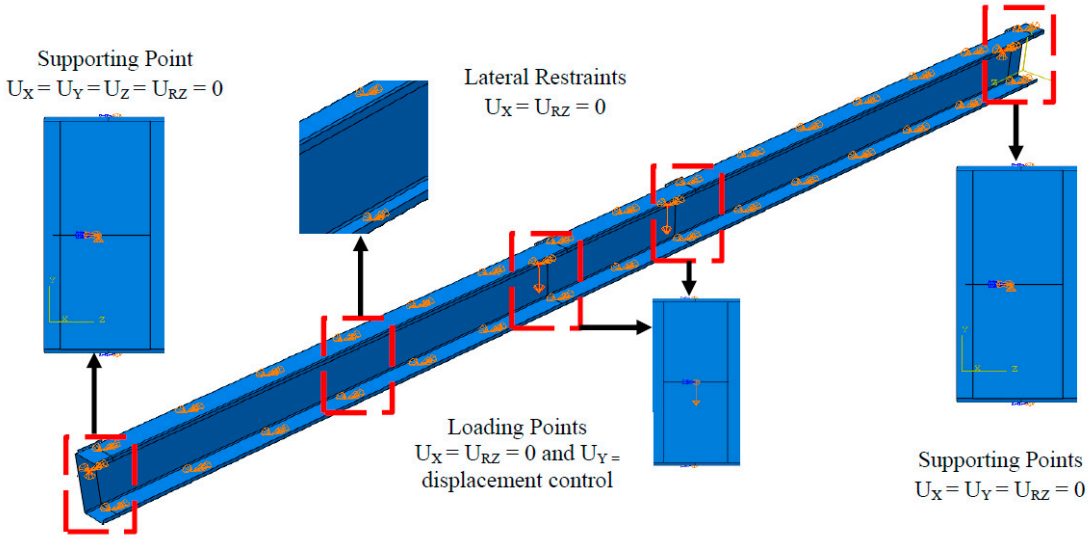

Figure 7. Boundary conditions of single sections.

2.4. Interaction and Properties

Web areas of the cross-sections considered are overlapped when combined to generate built-up sections which were incorporated using contact pairs. The interaction between

both sections was adopted with the surface-to-surface discretisation method. Following that, tangential and normal interaction properties were assigned to the relevant contact model, while frictionless formulation employed to the tangential behaviour "HARD" contact pressure-overclosure was adopted to the normal behaviour. Also, separation was allowed after contact in the interaction properties in the normal direction. Since previous studies revealed that failures occurred in the built-up beams before occurring in the screws, modelling of screws replicated with MPC connector section methods. A similar method was also observed in most of the numerical studies [31]. Nodes in both the beam corresponding to the screw locations were connected and created as a wire feature in the ABAQUS.

2.5. Solution Scheme

The flexural behaviour of these sections was assessed using buckling analysis and non-linear analysis, which were employed to observe the geometric imperfection and flexural behaviours, respectively. According to the previous studies 'Static General' and 'Static Riks' steps can be adopted in the non-linear analysis. Also, Yu and Schafer [32] and Schafer et al. [33] mentioned that static general scheme is a much more efficient method of predicting the ultimate capacity with post-buckling behaviour. Other researchers also used the same solution scheme in their studies [34]. Following a proper validation, a parametric study was conducted using the static general solution scheme. In the buckling analysis, the step was replaced with linear perturbation.

3. Validation and Parametric Plan

3.1. Validation of FE Models

Various experimental studies considering different cross-sections were verified using numerical studies in terms of moment capacity, failure mode and failure curve. The validation was conducted on Wang and Young's studies, who investigated the flexural behaviour of built-up open channel sections [13] and innovative sections with intermediate stiffeners [1,2] by accommodating four-point bending tests. Altogether, twelve experimental data were validated in this study. Table 3 presents the experimental to numerical moment capacity comparison. Mean and coefficient of variation (COV) values were calculated for moment proportion of experimental and numerical values. The mean and COV were 0.97 and 0.05, respectively, which closely coincide with experimental results.

Failure modes obtained for experimental studies are shown in Figures 8 and 9, together with the failure modes derived from numerical analyses. The failure modes were observed for OT1.9-136-S150, OT1.9-136-S300 and OT1.9-136-S600, open built-up channel sections and OV-0.48-B4 and OI-1.0-B4, which are open built-up sections with intermediate stiffeners and shown in the Figures 8 and 9, respectively. As can be seen in the failure mode comparison, the failure modes obtained from the FE modelling mirror very closely those of experimental failure modes.

Table 3. Moment capacity comparison between experimental and numerical analyses.

No.	Specimen	Reference	Test	Failure Mode Observed in Experimental	FE	Failure Mode Observed in Numerical	M_{Exp}/M_{FE}
			M_{Exp} (kNm)		M_{FE} (kNm)		
1	OT0.42-86-S75	[13]	1.206	D + L	1.294	D + L	0.93
2	OT0.42-86-S300		1.222	D + L	1.321	D + L	0.93
3	OT1.2-86-S75		7.417	D + L	7.230	D + L	1.03
4	OT1.2-86-S75R1		7.303	D + L	7.062	D + L	1.03
5	OT1.2-86-S75R1-R		7.341	D + L	7.012	D + L	1.05
6	OT1.2-86-S300		7.030	D + L	7.366	D + L	0.95
7	OT1.2-136-S150		12.240	D + L	12.378	D + L	0.99
8	OV-0.48-B4	[1,2]	1.246	L + F	1.335	L + F	0.93
9	OV-1.0-B4		4.238	L + F	4.385	L + F	0.97
10	OI-0.48-B4		1.880	L + F	2.088	L + F	0.90
11	OI-1.0-B4		6.092	D + F	6.180	D + F	0.99
12	OI-1.2-B4		7.208	D + F	8.018	D + F	0.90
			Mean				0.97
			COV				0.05

Note: D-Distortional buckling, L-Local buckling and F-Flexural buckling.

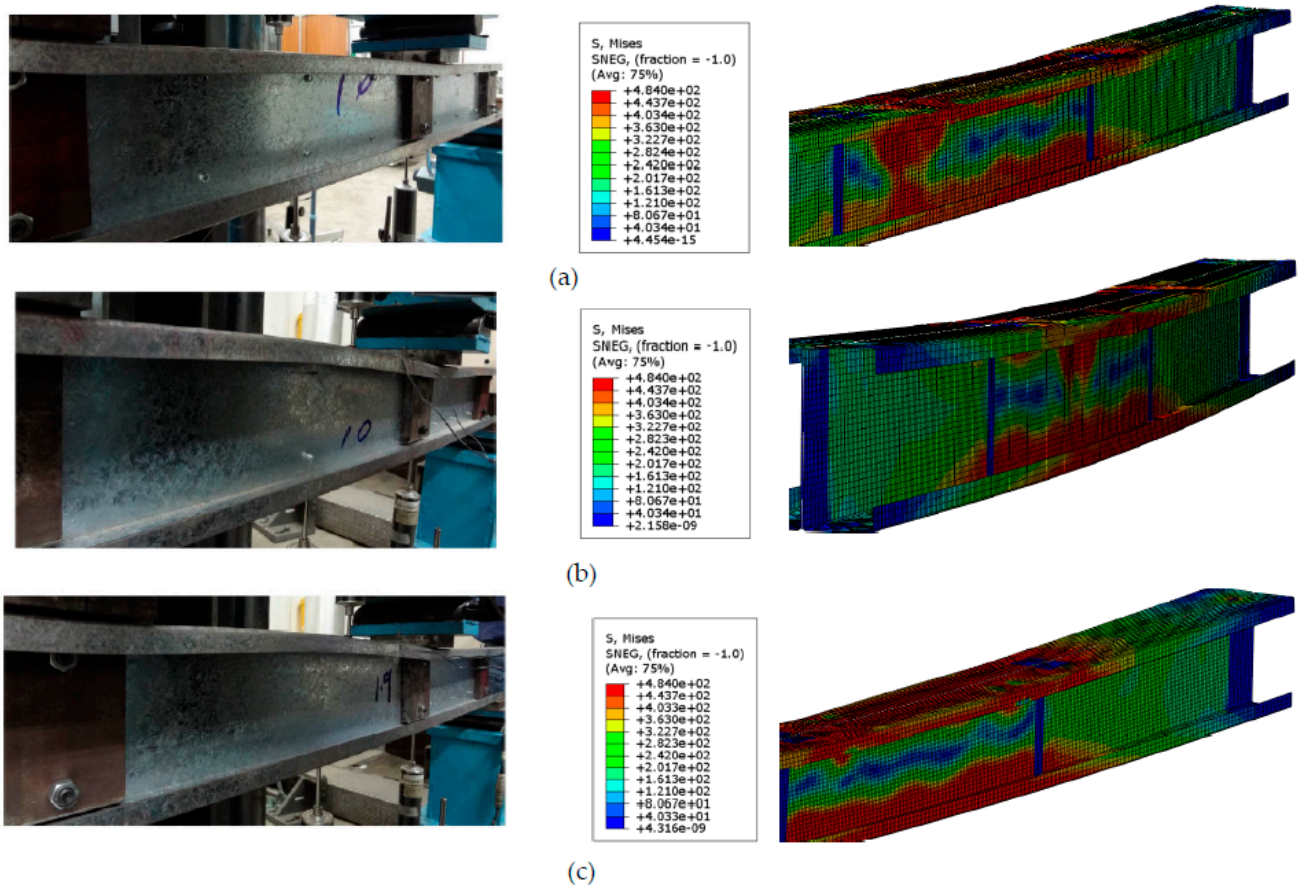

Figure 8. Failure mode comparison for (**a**) OT1.9-136-S150, (**b**) OT1.9-136-S300 and (**c**) OT1.9-136-S600 built-up channel section [13].

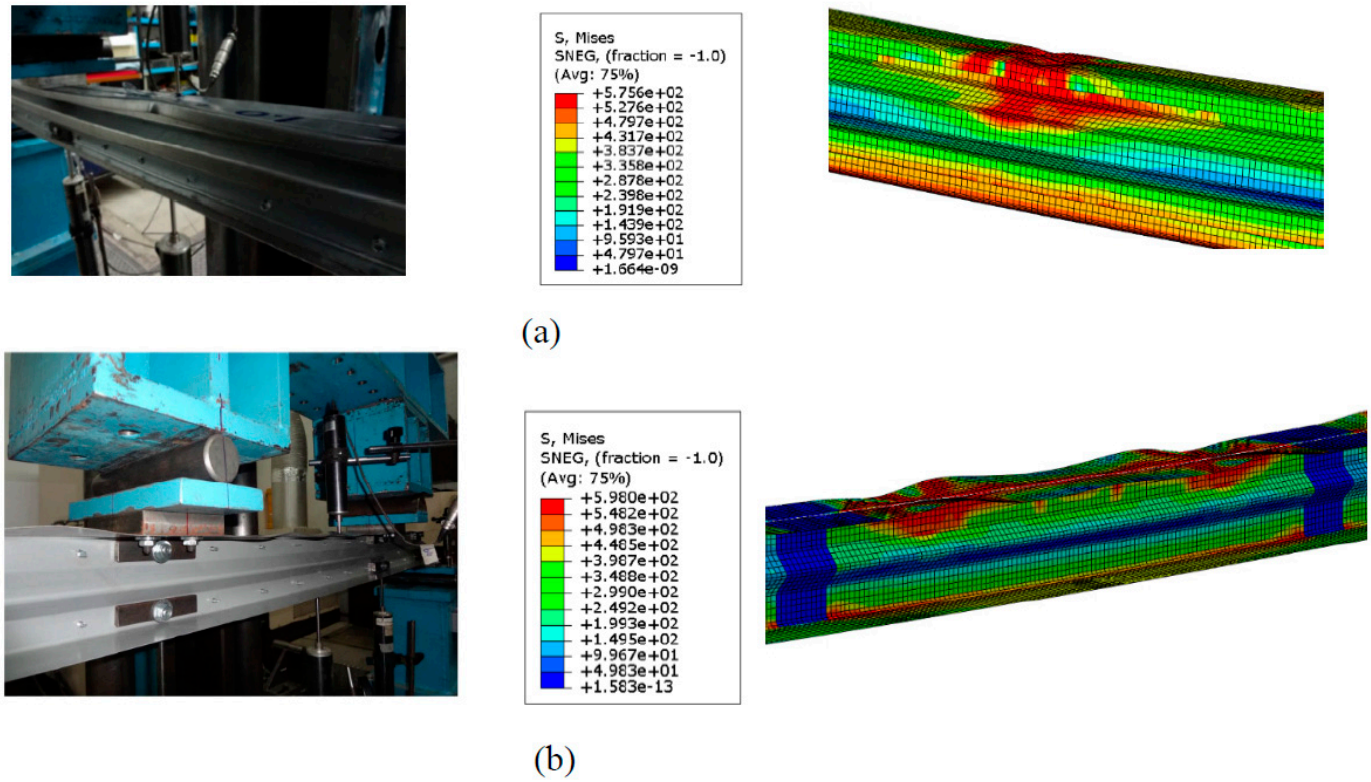

Figure 9. Failure mode comparison for (**a**) OI-1.0-B4 and (**b**) OV-0.48-B4 built-up channel sections with stiffeners [1,2].

Finally, moment-deflection curves derived in the experimental results were compared with the curve derived from numerical models and are presented in Figure 10. Curve comparison was conducted for open built-up sections OT1.2-136-S150 and OT1.2-86-S300, and ABAQUS predicted the best agreement with their experimental counterparts.

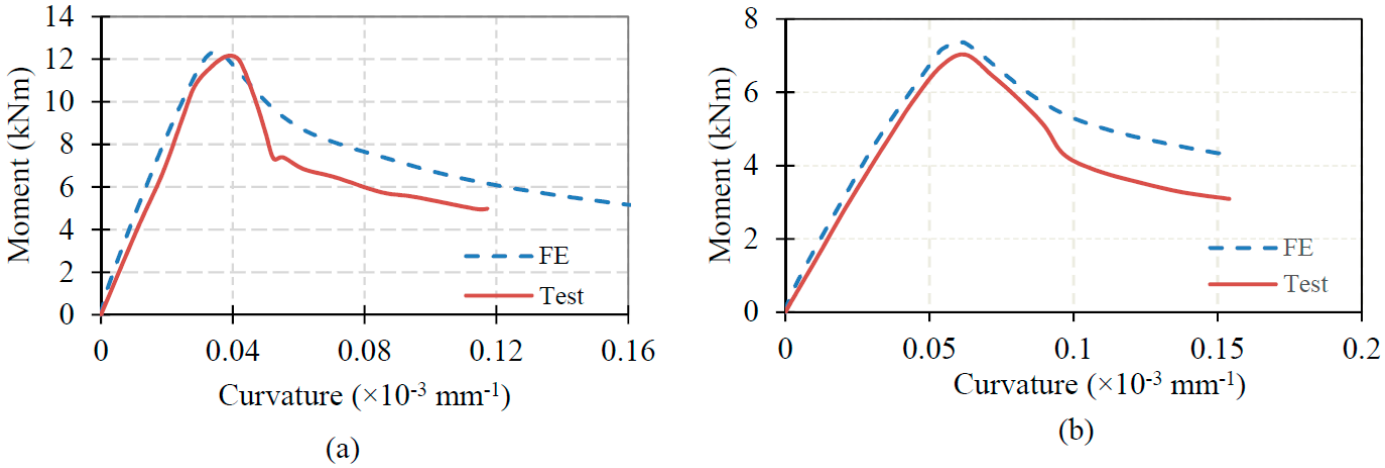

Figure 10. Failure curve comparison for (**a**) OT1.2-136-S150 (**b**) OT1.2-86-S300 [13].

3.2. Parametric Plan

The parametric plan was modelled accordingly to allow different materials, and different types of sections to analyse the results of each section, and materials to cover various aspects of construction requirements. Hence, four different sections, namely the benchmark section, optimised-LCB, folded-flange and super-sigma, were selected considering their better structural performances compared to conventional sections [11].

CFS, CF aluminium and CF stainless steel were selected as materials for this study. CFS is a highly rated material in the construction industry due to its benefits such as high strength-to-weight ratio, flexibility, lightweight compared hot-rolled sections and durability. Similarly, CF aluminium sections offer corrosion resistance, ease of fabrication, aesthetic desirability and lightweight and CF stainless steel sections provide high strength, corrosion resistance and ductility. Applications of all three materials remain in various places in the market, depending on their features. Since the above-mentioned materials are in higher demand in the construction market, all three materials were considered in the parametric studies. Two yield strengths (220 MPa and 450 MPa) were considered for CFS sections. Even though many types of aluminium and stainless-steel sections are available in the industry, two types of each material (Aluminium-H14 and H48, Stainless steel-1.4307 and 1.4362) were selected for comparative purposes. Moreover, both single sections and built-up sections were considered in the parametric study to check the amount of increment in the flexural performance of built-up sections compared to that of single sections. Therefore, overall, 48 numerical models were selected, consisting of all chosen sections and materials. Whilst Table 4 displays the opted parametric plan for the investigation, Table 5 shows the dimension details of selected sections. The details are illustrated in Figure 11.

Table 4. Parametric plan of numerical investigation.

Section Types	Sections	Materials	Material Classifications
Single	LCB-benchmark, Optimised-LCB, Super-Sigma, Folded-Flange	CFS	f_y = 220 MPa f_y = 450 MPa
		CF aluminium	H14 H48
		CF stainless steel	1.4307 1.4367
Built-up	LCB-benchmark, Optimised-LCB, Super-Sigma, Folded-Flange	CFS	f_y = 220 MPa f_y = 450 MPa
		CF aluminium	H14 H48
		CF stainless steel	1.4307 1.4367

Table 5. Dimension details of selected sections.

Parameters / Sections	h (mm)	b (mm)	c (mm)	d (mm)	W_1 (mm)	W_2 (mm)	W_3 (mm)	δ_1 (°)	δ_2 (°)
Benchmark	231	75	17	-	-	-	-	-	-
Optimised-LCB	269	50	23	-	-	-	-	-	-
Folded-Flange	185	48	50	17	-	-	-	105	95
Super-Sigma	270	50	17.5	-	41	30	139	34	-

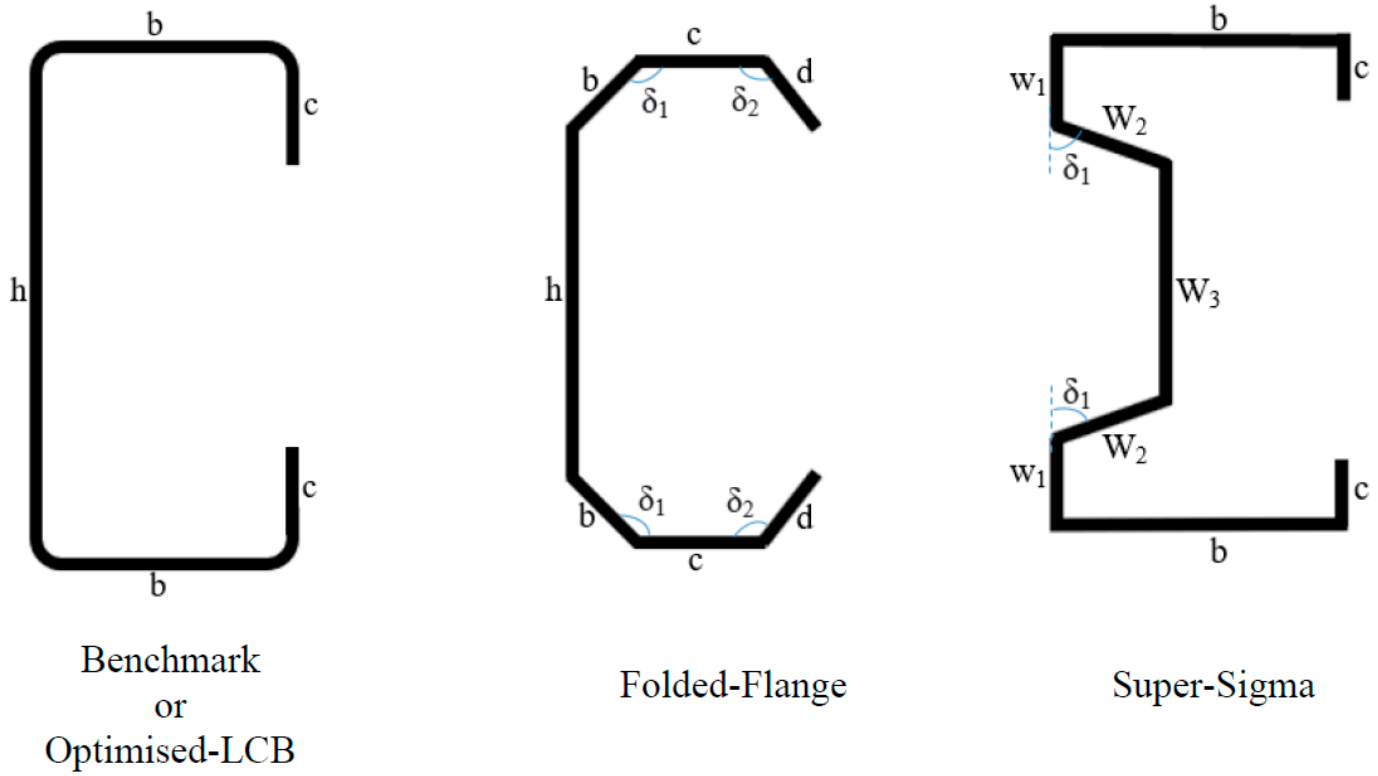

Figure 11. Illustration of selected section profiles.

4. Results and Discussion

The flexural behaviour of built-up sections was investigated, based on the numerical results obtained from the parametric studies. Tables 6 and 7 summarise the obtained numerical results for both built-up sections and single sections, respectively. In addition, Figures 12 and 13 depict how each built-up sections fail under a four-point bending case with time (A—initial stage, B—Before ultimate stage, C—During ultimate stage and D—Post-ultimate stage). Furthermore, the results obtained were analysed comparatively in three categories, namely material types, section types and comparison with single sections.

Table 6. Bending moment capacity for built-up sections.

Material	**CFS**		**AL**		**SS**	
Sections	f_y = 220 MPa	f_y = 450 MPa	H14	H48	1.4307	1.4362
Benchmark	16.05	24.60	6.30	7.35	16.05	25.50
Optimised-LCB	16.55	29.10	7.80	8.55	16.65	32.40
Folded-Flange	18.45	39.45	12.90	15.75	21.00	43.35
Super-Sigma	13.50	*NA	8.70	11.25	16.80	34.50

Note: *NA—Not available due to numerical issues.

Table 7. Bending moment capacity for single sections.

Material	**CFS**		**AL**		**SS**	
Sections	f_y = 220 MPa	f_y = 450 MPa	H14	H48	1.4307	1.4362
Benchmark	5.40	10.41	2.10	2.55	6.00	12.45
Optimised-LCB	7.35	13.28	3.00	3.60	7.65	14.85
Folded-Flange	7.80	16.60	3.90	4.65	8.70	18.75
Super-Sigma	6.30	14.90	2.70	3.45	7.35	15.45

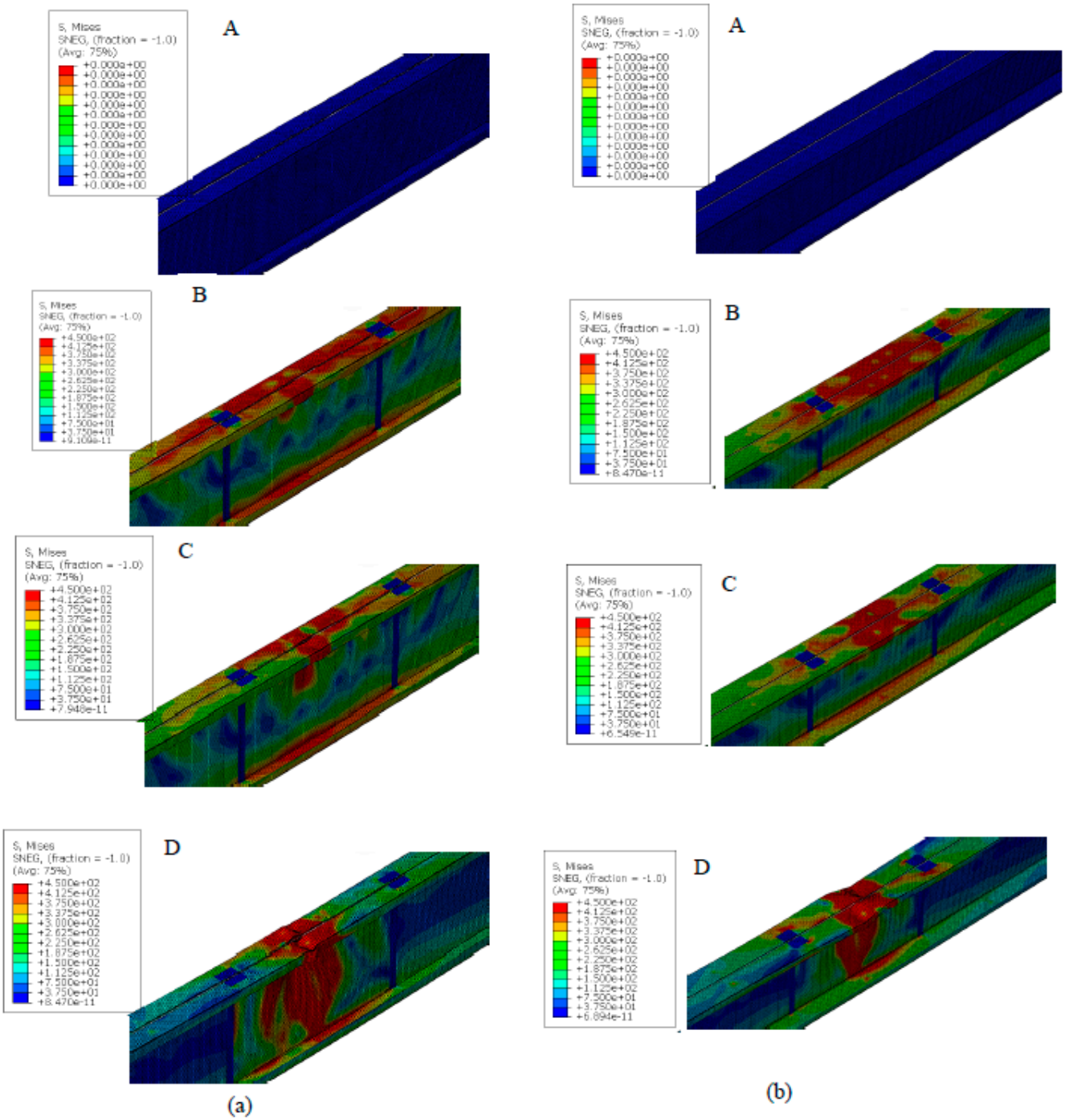

Figure 12. Failure patterns of built-up sections: (**a**) LCB-benchmark; (**b**) Optimised-LCB.

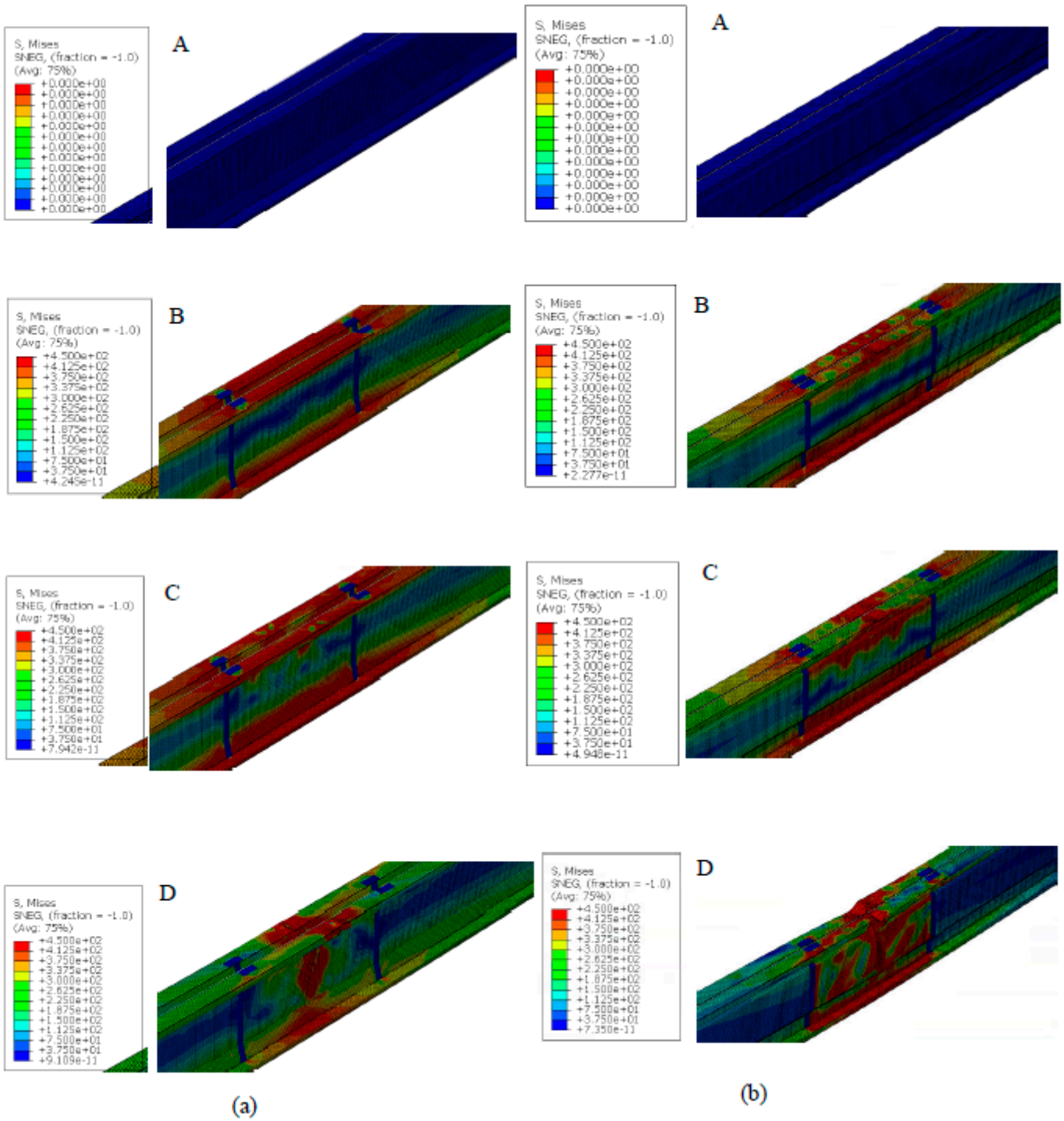

Figure 13. Failure patterns of built-up sections: (**a**) Folded-Flange; (**b**) Super-Sigma.

With regards to the built-up sections, maximum bending capacity enhancement was obtained for folded-flange built-up sections compared to their single sections for all three materials except CFS with grade of 220 MPa and CFS stainless steel with 1.4307, where the benchmark section showcased a higher increment. Increment in the flexural strength of studied built-up section for CFS grade of 220 MPa varies from 114% (super-sigma) to 197% (benchmark), whilst variation lies between 119% (optimised-LCB) and 137% (folded-flange) for CFS with 450 MPa. For aluminium, the increment pattern was similar and variation in the amount of increment for H14 and H48 was 160% to 230% and 137% to 238%, respectively, and the minimum increment was in optimised-LCB, while folded-flange

obtained the maximum. Finally, the increment in stainless steel for 1.4307 and 1.4362 varied between 117% (optimised-LCB) and 167% (folded-flange), and 104% (benchmark) and 131% (folded-flange), respectively. The results proved, therefore, that folded-flange exhibits the highest increment compared to the other cross-sections considered, illustrated in Figure 14. The fraction of increment in the capacity of the built-up section compared to single section was calculated and it was observed that it was more than twice as much, and was up to 3.4 times for folded-flange sections.

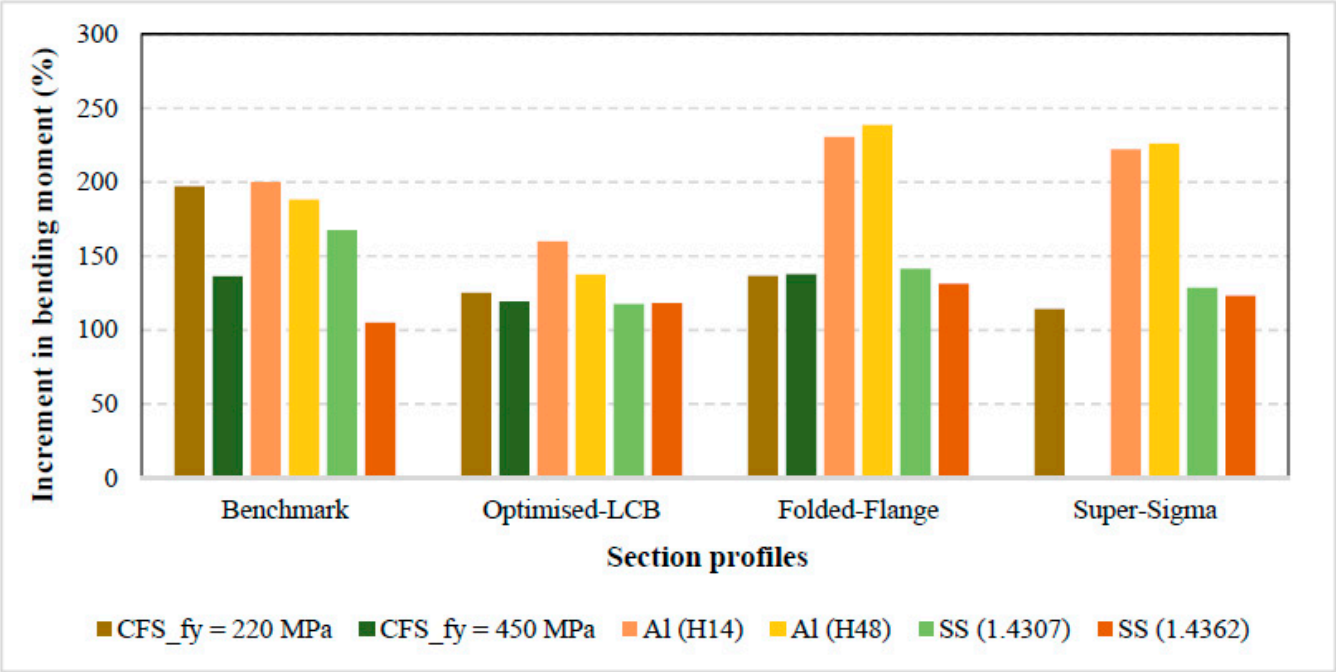

Figure 14. Bending capacity increment comparison between built-up and single sections based on different cross-sections.

Based on the material properties selected for parametric study, CFS carbon with a grade of 220 MPa, aluminium with H48 (fy = 220 MPa) and stainless steel with 1.4307 (fy = 220 MPa) had similar material grades and comparison in the flexural strength increment was observed in the above-mentioned properties for all cross-sections (Figure 15). For benchmark sections, the highest increment was observed as 197% in CFS, while super-sigma sections showcased better capacity increment (137%) with aluminium. Also, minimum increments of 104% for benchmark and 114% for super-sigma were observed in stainless steel and CFS, respectively. However, optimised-LCB and folded-flange predicted a similar pattern in the increment of flexural behaviour of built-up sections compared to that of single sections, and maximum increment was obtained for aluminium, whilst stainless steel predicted the least. It can be concluded, therefore, that the performance of benchmark built-up sections is better with CFS and the remaining built-up sections: optimised-LCB, folded-flange and super-sigma will provide greater strength with aluminium.

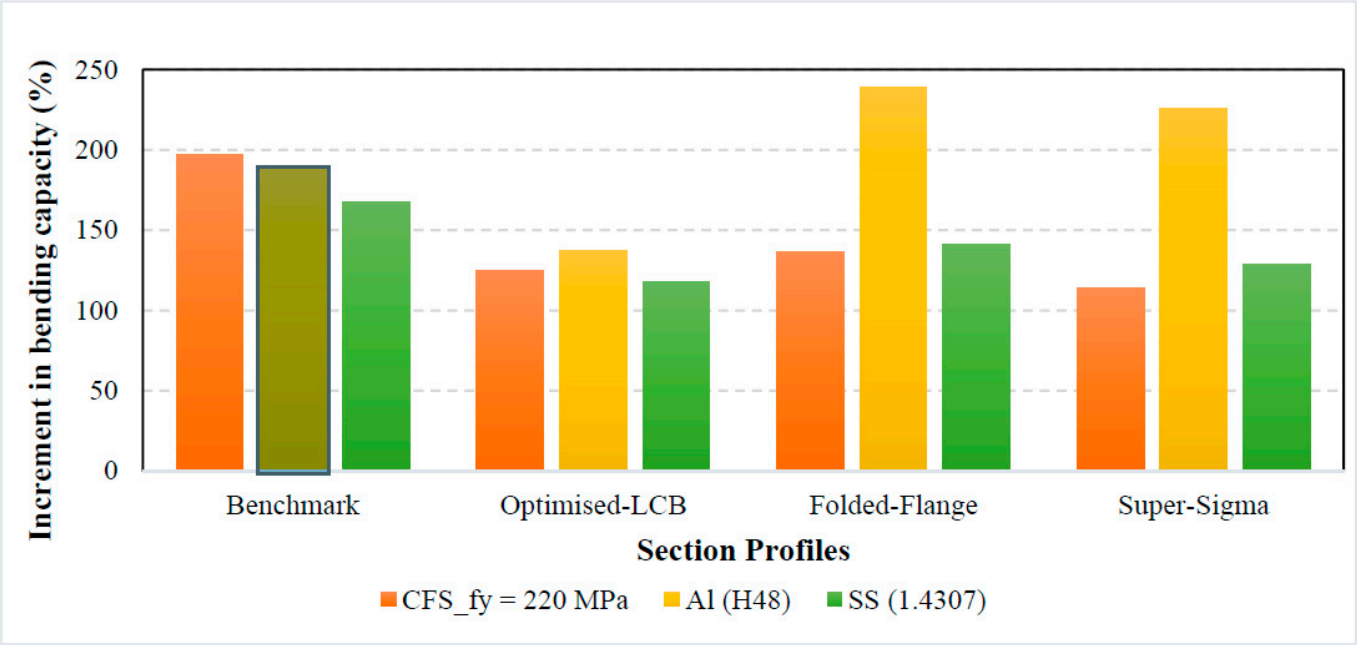

Figure 15. Bending capacity increment comparison for similar strength of different materials.

Moreover, bending moment capacity increment fraction of optimised-LCB, folded-flange and super-sigma sections was calculated based on the bending moment capacity of benchmark section and illustrated in Figure 16. The bending moment capacity of benchmark section was considered as 1 and the increment of other sections was calculated based on it. For single sections, the bending moment capacity increment of the folded-flange section was higher than other sections with all six considered material properties. The fraction increment was observed from 1.44 (for material property of CFS_fy = 220 MPa) to 1.86 (for material property of SS (1.4362)). The second increment was then observed for the optimised-LCB expect with the material property of CFS_fy = 450 MPa and SS (1.4362), in which the super-sigma section recorded the second highest capacity. Also, the bending moment capacity of optimised-LCB, folded-flange and super-sigma sections was greater than the benchmark section. The benchmark section was therefore the lowest in the ranking of bending moment capacity of single sections. According to Figure 16b, the increment fraction of the folded-flange section again recorded the highest increment for built-up sections. The increment fraction fell between 1.15 (for material property of CFS_fy = 220 MPa) and 2.14 (for material property of Al (H48)). Second highest and third highest increments were observed in the super-sigma and optimised-LCB sections for the material properties of Al (H14), Al (H48) and SS (1.4362). However, both the super-sigma and optimised-LCB sections showcased almost similar increment for the material property of SS (1.4307). The bending moment capacity increment fraction of super-sigma section was less than 1.0 for the material property of CFS_fy = 220 MPa.

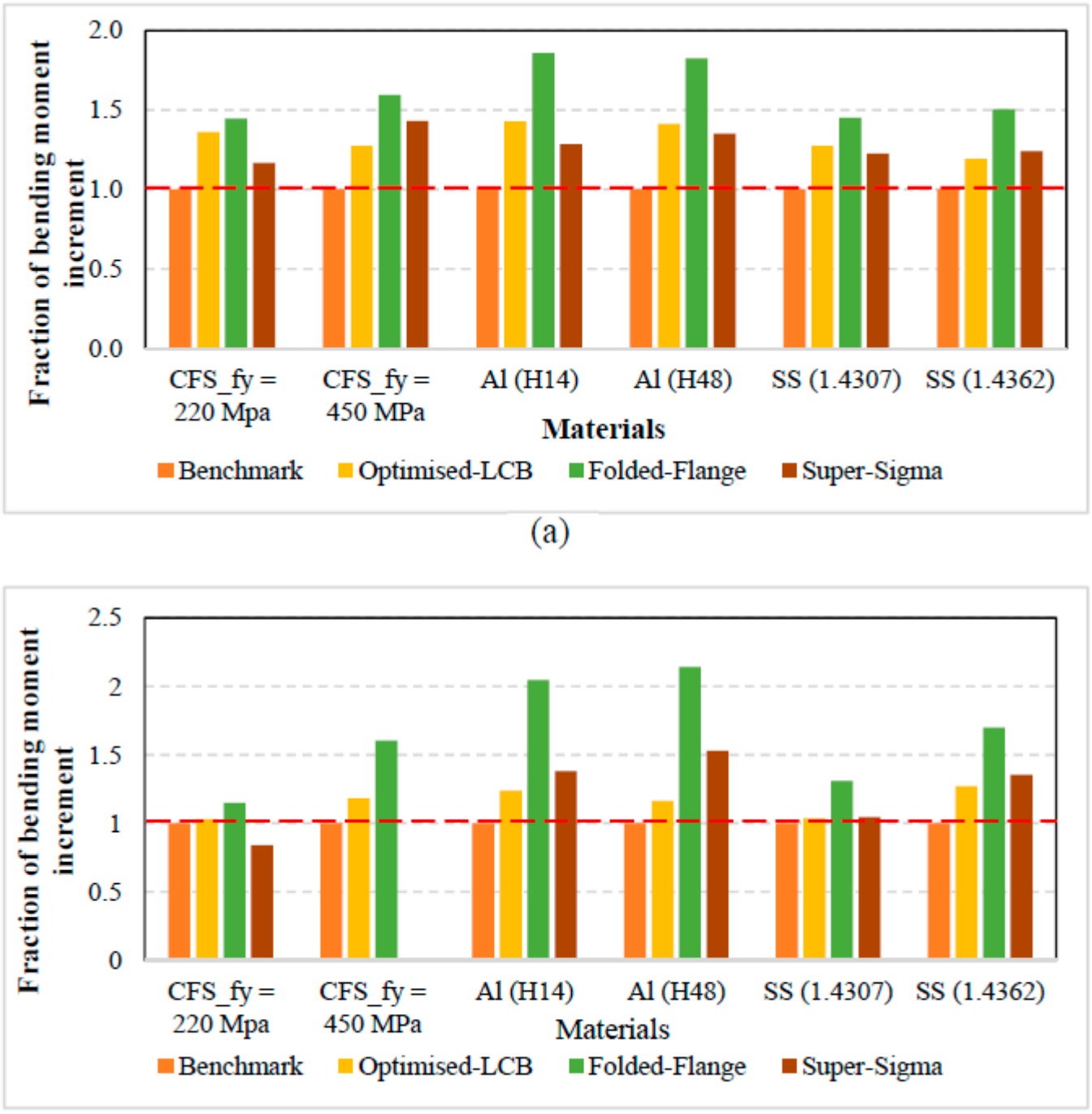

Figure 16. Bending moment capacity increment for different (**a**) single and (**b**) built-up sections based on benchmark section.

Overall, aluminium sections performed better in terms of flexural capacity compared to CFS and stainless steel, whilst folded-flange sections showcased better bending capacity compared to the other four sections considered in this study. Moreover, built-up sections of these optimised sections performed better under flexural tests and attained greater bending capacity, corresponding to their single sections. Therefore, these sections can be used in the building industry to gain maximum design bending capacities and to meet their requirements. A detailed parametric study is planned in the future to propose design equations and to apply them in engineering applications.

5. Ongoing and Future Works

The aim of this study is to introduce the built-up sections made up of optimised profiles to the modular building industry to attain their structural requirements in terms of longer span beams and light-weight modules. The authors carried out a review study in this paper to investigate different profiles with three different materials, namely CFS, CF aluminium and CF stainless steel by considering their demands and benefits to the construction industry. The authors are also actively working on several other different cross-sections to investigate their structural behaviours in terms of web crippling, shear and flexural and to propose the best among them. At that stage, full-scale experimental and numerical tests will be carried out for specific sections, and design equations will be proposed for modular building applications.

6. Conclusions

This study reports the results from the numerical analysis carried out to examine the bending behaviour of built-up sections composed of optimised sections such as benchmark, super-sigma, folded-flange and optimised-LCB with three different selected materials, namely CFS, CF aluminium and CF stainless steel. Accordingly, the parametric plan was well-developed, comprising all varying parameters including materials, yield strength and section types. Earlier, the numerical simulation method was validated with experimental studies and the parametric studies were carried out. The simulation results were recorded for single sections and built-up sections and the outcomes were compared with individual sections and built-up sections, considering all different materials as well as the sections. The comparison indicated that all built-up sections composed of benchmark, super-sigma, folded-flange and optimised-LCB showcased flexural capacity enhancement from 99% to 238% for all three materials. Meanwhile, significant capacity improvement was observed for single and built-up sections composed of both super-sigma and folded-flange sections compared to the other two sections. However, by a slight margin, the folded-flange section topped the table based on flexural capacity as well as the percentage of increment, compared to the single section which was a maximum of 238% with aluminium. Hence, this paper strongly recommends folded-flange built-up sections in structural applications to attain more benefits in terms of structural capacity as well as stiffness.

Author Contributions: Conceptualization, K.P. and K.R.; methodology, E.K. and J.H.; software, E.K. and K.T.; validation, K.T.; formal analysis, E.K., J.H. and K.T.; data curation, J.H.; writing—original draft preparation, E.K., J.H., K.T. and T.S.; writing—review and editing, K.P., K.R. and G.B.G.A.; visualization, K.P.; supervision, K.P. All authors have read and agreed to the published version of the manuscript.

Funding: This research received no external funding.

Institutional Review Board Statement: Not applicable.

Informed Consent Statement: Not applicable.

Data Availability Statement: Not applicable.

Acknowledgments: The authors would like to acknowledge Northumbria University, The Home Engineers and the European Research Council for their support in conducting this research study.

Conflicts of Interest: The authors declare no conflict of interest.

References

1. Wang, L.; Young, B. Behavior of Cold-Formed Steel Built-Up Sections with Intermediate Stiffeners under Bending. II: Parametric Study and Design. *J. Struct. Eng.* **2016**, *142*, 04015151. [CrossRef]
2. Wang, L.; Young, B. Behavior of Cold-Formed Steel Built-Up Sections with Intermediate Stiffeners under Bending. I: Tests and Numerical Validation. *J. Struct. Eng.* **2016**, *142*, 04015150. [CrossRef]
3. Li, Q.-Y.; Young, B. Experimental study on cold-formed steel built-up section beam-columns experiencing non-uniform bending. *Eng. Struct.* **2022**, *256*, 113954. [CrossRef]

4. Laím, L.; Rodrigues, J.P.C.; Craveiro, H.D. Flexural behaviour of beams made of cold-formed steel sigma-shaped sections at ambient and fire conditions. *Thin-Walled Struct.* **2015**, *87*, 53–65. [CrossRef]
5. Lu, Y.; Zhou, T.; Li, W.; Wu, H. Experimental investigation and a novel direct strength method for cold-formed built-up I-section columns. *Thin-Walled Struct.* **2017**, *112*, 125–139. [CrossRef]
6. Li, Q.-Y.; Young, B. Design of cold-formed steel built-up open section members under combined compression and bending. *Thin-Walled Struct.* **2022**, *172*, 108890. [CrossRef]
7. Thirunavukkarasu, K.; Kanthasamy, E.; Gatheeshgar, P.; Poologanathan, K.; Rajanayagam, H.; Suntharalingam, T.; Dissanayake, M. Sustainable Performance of a Modular Building System Made of Built-Up Cold-Formed Steel Beams. *Buildings* **2021**, *11*, 460. [CrossRef]
8. Thirunavukkarasu, K.; Kanthasamy, E.; Poologanathan, K.; Tsavdaridis, K.D.; Gatheeshgar, P.; Hareindirasarma, S.; McIntosh, A. Shear performance of SupaCee sections with openings: Numerical studies. *J. Constr. Steel Res.* **2022**, *190*, 107142. [CrossRef]
9. Keerthan, P.; Mahendran, M. Elastic shear buckling characteristics of LiteSteel beams. *J. Constr. Steel Res.* **2010**, *66*, 1309–1319. [CrossRef]
10. Keerthan, P.; Mahendran, M. Experimental investigation and design of lipped channel beams in shear. *Thin-Walled Struct.* **2015**, *86*, 174–184. [CrossRef]
11. Gatheeshgar, P.; Poologanathan, K.; Gunalan, S.; Nagaratnam, B.; Tsavdaridis, K.D.; Ye, J. Structural behaviour of optimized cold-formed steel beams. *Steel Constr.* **2020**, *13*, 294–304. [CrossRef]
12. Pham, C.H.; Bruneau, L.A.; Hancock, G.J. Experimental Study of Longitudinally Stiffened Web Channels Subjected to Combined Bending and Shear. *J. Struct. Eng.* **2015**, *141*, 4015018. [CrossRef]
13. Wang, L.; Young, B. Behaviour and design of cold-formed steel built-up section beams with different screw arrangements. *Thin-Walled Struct.* **2018**, *131*, 16–32. [CrossRef]
14. Anbarasu, M. Simulation of flexural behaviour and design of cold-formed steel closed built-up beams composed of two sigma sections for local buckling. *Eng. Struct.* **2019**, *191*, 549–562. [CrossRef]
15. Ye, J.; Mojtabaei, S.M.; Hajirasouliha, I.; Shepherd, P.; Pilakoutas, K. Strength and deflection behaviour of cold-formed steel back-to-back channels. *Eng. Struct.* **2018**, *177*, 641–654. [CrossRef]
16. Jeyaragan, S.; Mahendran, M. Numerical Modelling and Design of the New Built-up LiteSteel Beams. In Proceedings of the Fifth International Conference on Coupled Instabilities in Metal Structures CIMS, Sydney, Australia, 23–25 June 2008.
17. Xu, L.; Sultana, P.; Zhou, X. Flexural strength of cold-formed steel built-up box sections. *Thin-Walled Struct.* **2009**, *47*, 807–815. [CrossRef]
18. Wang, L.; Hu, M.; Young, B. Tests of aluminum alloy perforated built-up sections subjected to bending. *Thin-Walled Struct.* **2021**, *158*, 107136. [CrossRef]
19. Karthik, C.; Anbarasu, M. Cold-formed ferritic stainless steel closed built-up beams: Flexural behaviour and numerical parametric study. *Thin-Walled Struct.* **2021**, *164*, 107816. [CrossRef]
20. *EN 1993-1-3*; Eurocode3: Design of Steel Structures, Part1.3: General Rules—Supplementary Rules for Coldformed Steel Members and Sheeting. European Committee for Standardization: Brussels, Belgium, 2005.
21. SIMULIA. *ABAQUS Standard User's Manual*; Version 6.14; Dassault Systèmes Simulia Corp.: Johnston, RI, USA, 2013.
22. Poologanathan, K.; Mahendran, M. Numerical modelling and design of lipped channel beams subject to shear. In Proceedings of the European Conference on Steel and Composite Structures, Naples, Italy, 10–12 September 2014; pp. 445–446.
23. Poologanathan, K.; Mahendran, M. Numerical modeling of litesteel beams subject to shear. *J. Struct. Eng.* **2011**, *137*, 1428–1439.
24. Keerthan, P.; Mahendran, M. Shear buckling characteristics of cold-formed steel channel beams. *Int. J. Steel Struct.* **2013**, *13*, 385–399. [CrossRef]
25. Su, M.-N.; Young, B.; Gardner, L. Testing and Design of Aluminum Alloy Cross Sections in Compression. *J. Struct. Eng.* **2014**, *140*, 04014047. [CrossRef]
26. Alsanat, H.; Gunalan, S.; Poologanathan, K.; Guan, H. Web crippling investigations of aluminum lipped channel sections under one-flange loading conditions. *Thin-Walled Struct.* **2021**, *166*, 108025. [CrossRef]
27. McIntosh, A.; Kanthasamy, E.; Poologanathan, K.; Gunalan, S.; Gatheeshgar, P.; Corradi, M.; Higgins, C. Web crippling design of channel beams: Carbon steel, stainless steel and aluminium. *J. Constr. Steel Res.* **2022**, *196*, 107427. [CrossRef]
28. Rasmussen, K.J. Full-range stress–strain curves for stainless steel alloys. *J. Constr. Steel Res.* **2003**, *59*, 47–61. [CrossRef]
29. Cruise, R.B.; Gardner, L. Strength enhancements induced during cold forming of stainless steel sections. *J. Constr. Steel Res.* **2008**, *64*, 1310–1316. [CrossRef]
30. Ashraf, M.; Gardner, L.; Nethercot, D. Strength enhancement of the corner regions of stainless steel cross-sections. *J. Constr. Steel Res.* **2005**, *61*, 37–52. [CrossRef]
31. Wang, L.; Young, B. Design of cold-formed steel built-up sections with web perforations subjected to bending. *Thin-Walled Struct.* **2017**, *120*, 458–469. [CrossRef]
32. Yu, C.; Schafer, B.W. Simulation of cold-formed steel beams in local and distortional buckling with applications to the direct strength method. *J. Constr. Steel Res.* **2007**, *63*, 581–590. [CrossRef]
33. Schafer, B.; Li, Z.; Moen, C. Computational modeling of cold-formed steel. *Thin-Walled Struct.* **2010**, *48*, 752–762. [CrossRef]
34. Keerthan, P.; Mahendran, M.; Hughes, D. Numerical studies and design of hollow flange channel beams subject to combined bending and shear actions. *Eng. Struct.* **2014**, *75*, 197–212. [CrossRef]